Blood and Lymphatic Cancer: Targets and Therapy

Dovepress
Taylor & Francis Group

Open Access Full Text Article

ORIGINAL RESEARCH

Alantolactone Inhibits Double Expression Lymphoma via Dual-Targeted Glycogen Synthase Kinase 3 Beta and B-Cell Lymphoma2

Jianhua Chen[1,*], Qing Liao[1,2,*], Sha Yang[1], Jiaojiao Bian[1], Xianfu Li[3], Lu Zhao[4], Dan Wen[1], Dazhang Bai[5], Chunlei Yu[1], Chunyang Zhou[1], Zhengmin Xu[1,6]

[1]Department of Pharmacology Institute of Materia Medica, School of Pharmacy, North Sichuan Medical College, Nanchong, Sichuan, 637000, People's Republic of China; [2]Department of Pharmacy, Yingshan County People's Hospital, Nanchong, Sichuan, 637000, People's Republic of China; [3]Department of Radiotherapy, Nuclear Medicine Department, Affiliated Hospital of North Sichuan Medical College, Nanchong, Sichuan, 637000, People's Republic of China; [4]Sichuan Institute for Drug Control (Sichuan Testing Center of Medical Devices), Chengdu, Sichuan, 637000, People's Republic of China; [5]Department of Neurology, Affiliated Hospital of North Sichuan Medical College, Institute of Neurological Diseases, North Sichuan Medical College, Nanchong, Sichuan, 637000, People's Republic of China; [6]Key Laboratory of Traditional Chinese Medicine for Prevention and Treatment of Skeletal Muscle Disease, Nanchong Traditional Chinese Medicine Hospital, Nanchong, Sichuan, 637000, People's Republic of China

*These authors contributed equally to this work

Correspondence: Zhengmin Xu, North Sichuan Medical College, No. 234 Fuliang Road, Shunqing District, Nanchong, Sichuan, 637000, People's Republic of China, Email xuzhengmin@nsmc.edu.cn

Background: Dual-expression lymphoma (DEL) is an aggressive subtype with concurrent MYC and BCL2 overexpression. This disease exhibits a poor prognosis and responds poorly to standard R-CHOP therapy,highlighting the urgent need for novel treatments. Alantolactone (ALA), a natural compound, has shown anticancer potential, but its efficacy and mechanism in DEL remain unclear. This study aimed to investigate the anti-tumor effects of ALA against DEL and its underlying dual-targeting mechanism.

Methods: The cytotoxic activity of ALA was assessed in lymphoma cell lines and a normal lymphocyte line. Apoptosis was evaluated by flow cytometry and Western blotting. Network pharmacology, molecular docking, dynamics simulations, and cellular thermal shift assays (CETSA) were utilized to identify and validate direct targets of ALA. The anti-tumor efficacy of ALA was further examined in a DEL xenograft mouse model using PET-CT imaging and survival analysis.

Results: In the present study, the anticancer activity of ALA in DEL was explored in vivo and in vitro. ALA was shown to inhibit DEL growth in vivo with little toxicity to normal tissues. Mechanistically, ALA stabilized active glycogen synthase kinase 3β (GSK3β) (binding affinity: −15.66 kcal/mol; ΔTm +9°C), enhancing β-catenin degradation and suppressing Wnt-driven oncogenesis. Simultaneously, ALA directly bound BCL2 (−22.22 kcal/mol), triggering both intrinsic and extrinsic apoptotic pathways. Simultaneously, ALA directly bound BCL2 (binding affinity: −22.22 kcal/mol), triggering both intrinsic and extrinsic apoptotic pathways. ALA exhibited robust anti-DEL activity across preclinical models. While in vivo it significantly suppressed tumor progression (SUVmax reduction >50%, $p<0.01$) and extended survival (median 50 vs 80 days, $p<0.01$) in DEL xenografts. The therapeutic relevance was underscored by clinical correlation showing DEL patients with high GSK3β expression had superior survival outcomes.

Conclusion: ALA exerts potent anti-DEL activity by simultaneously targeting GSK3β in the Wnt pathway and directly inhibiting BCL2, leading to suppressed tumor proliferation and induced apoptosis. Our findings highlight ALA as a promising multi-targeting therapeutic candidate for DEL and propose a novel strategy against this refractory lymphoma.

Keywords: alantolactone, dual-expression lymphoma, Wnt, glycogen synthase kinase 3β, B-cell lymphoma 2, apoptosis

Introduction

Lymphomas represent 3.6% of global cancer burden, with diffuse large B-cell lymphoma (DLBCL) constituting the most common aggressive subtype in China.[1–3] While the prednisone, vincristine, doxorubicin and cyclophosphamide

Received: 29 July 2025
Accepted: 6 December 2025
Published: 12 December 2025

Graphical Abstract

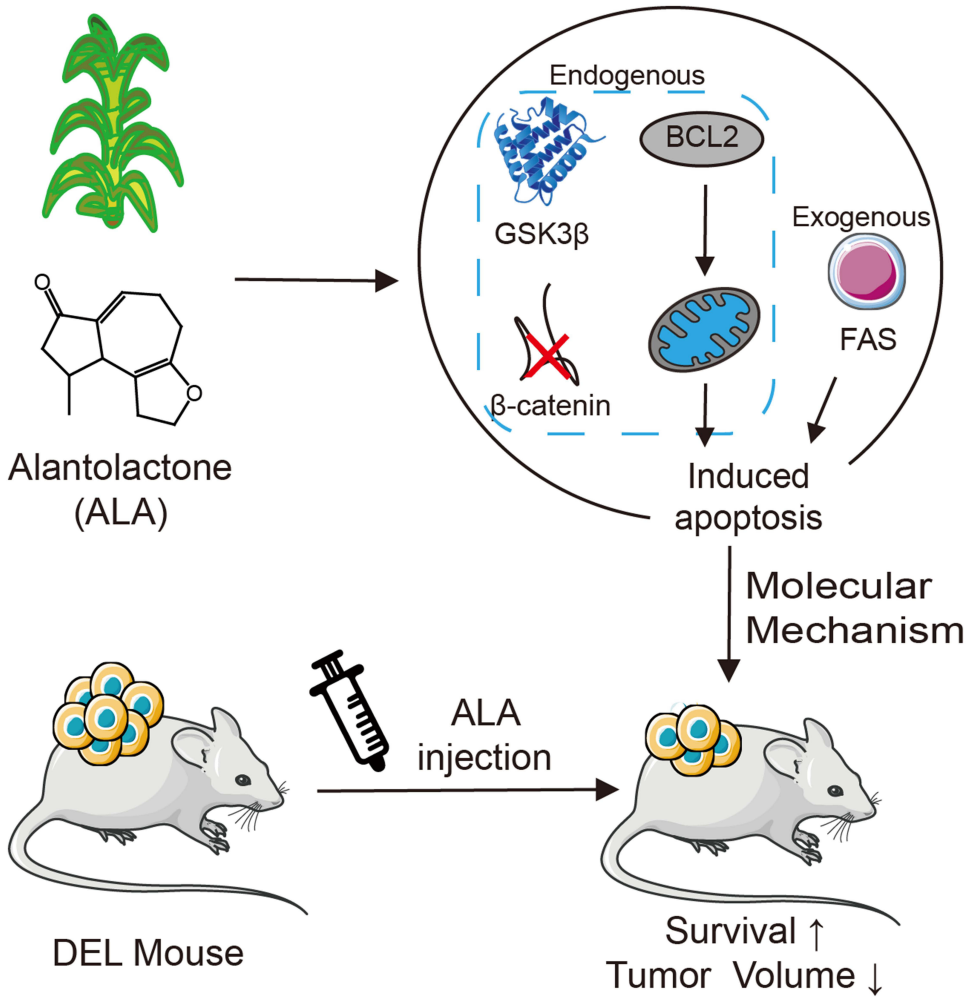

(R-CHOP) regimen achieves 60% 5-year survival in standard DLBCL,[4] The DEL subtype characterized by concurrent MYC and BCL2 overexpression and accounting for 20–30% of all DLBCL cases exhibits strikingly inferior outcomes, with a 5-year overall survival rate often below 30%.[5–7] This high prevalence and profound prognostic dichotomy underscore a significant unmet clinical need.

The pursuit of targeted therapies for DEL has been an area of intense translational focus, yet clinical progress has been limited. The pivotal Phase II Alliance A051701 trial tested the addition of the BCL2 inhibitor venetoclax to standard R-CHOP, aiming to overcome the apoptotic blockade conferred by BCL2 overexpression. Despite robust mechanistic rationale, this combination failed to improve progression-free or overall survival and instead increased hematologic and infectious toxicities.[8] The advent of immunotherapies including CD19-directed chimeric antigen receptor (CAR) T-cell therapy and bispecific antibodies (BsAbs) such as glofitamab and epcoritamab—has transformed the treatment landscape for relapsed or refractory (R/R) DLBCL. Nevertheless, their efficacy in DEL remains sub-optimal: response rates are lower, remissions shorter, and relapses more frequent than in non-DEL DLBCL.[8,9] Moreover, autologous stem cell transplantation (ASCT) offers only transient benefit in chemosensitive DEL, with progression-free survival markedly inferior to that in non-DEL cases.[10] Together, these findings underscore the urgent need for novel therapeutic strategies in DEL. At the molecular level, DEL is characterized by the co-activation of MYC and BCL2, resulting in unchecked proliferation coupled with impaired apoptosis. Direct pharmacologic inhibition of MYC remains

a formidable challenge due to its intrinsically disordered structure and lack of druggable domains.[11] Consequently, attention has shifted toward indirect approaches to destabilize or suppress MYC activity. In MYC-driven lymphomas, GSK3β functions as a tumor suppressor by phosphorylating MYC at threonine 58, promoting ubiquitin-mediated proteasomal degradation.[11,12] Notably, GSK3β exhibits context-dependent roles across malignancies, acting as either a tumor suppressor or oncogene depending on cellular context[13] In prostate cancer, for instance, the long non-coding RNA LINC00908 upregulates GSK3β to promote β-catenin degradation and suppress Wnt pathway signaling.[14] Conversely, pharmacologic inhibition of GSK3β has demonstrated therapeutic benefit in adult T-cell leukemia/lymphoma (ATLL).[15] In DLBCL, exosomal ENO2 promotes tumor progression through the GSK3β/β-catenin/c-Myc signaling pathway.[16] Collectively, these findings position DLBCL, and particularly its DEL subtype, Restoring or stabilizing GSK3β therefore represents a mechanistically rational precision oncology strategy.

The Wnt/β-catenin pathway is a central regulator of proliferation and survival, and its aberrant activation contributes to lymphomagenesis. GSK3β negatively regulates this pathway by phosphorylating β-catenin, leading to its degradation.[17] Hence, pharmacologic agents that preserve or enhance GSK3β activity may concurrently suppress Wnt-driven oncogenic programs, providing a convergent strategy in DEL.

In parallel, DEL is characterized by resistance to apoptosis due to BCL2 overexpression. BCL2 sequesters pro-apoptotic proteins such as BAX and maintains mitochondrial membrane integrity. While venetoclax has achieved success in chronic lymphocytic leukemia, its efficacy in DLBCL-particularly DEL has been limited.[18] Effective therapeutic intervention in DEL will thus require concurrent disruption of proliferative signaling and apoptotic resistance.

Natural products continue to serve as valuable sources of multi-target anticancer agents capable of modulating interconnected signaling networks. ALA, a plant-derived sesquiterpene lactone, has demonstrated broad antitumor activity across multiple malignancies.[19–23] However, its potential against DEL remains unexplored. DEL represents an aggressive molecular phenotype with poor response to standard chemo-immunotherapy and limited targeted options. Investigating whether ALA can suppress DEL and explore the potential mechanism therefore addresses a clear therapeutic void.

Materials and Methods

Cell Culture

Human lymphoma cell lines (Kasumi-6, Namalwa, SUDHL-4, SUDHL-6, Raji and Ramos) and a murine normal B lymphocyte cell line (Baf3) were gifted by CCLab, State Key Laboratory of Sichuan University. The cell lines were validated by short tandem repeat analysis using the Goldeneye™ DNA ID System 20A Assay (Peoplespot, Beijing). For all experiments, cells were used within 10 passages. The cells were cultured in 6-well plates (NEST, Wuxi, China) using RPMI1640 medium (Biosharp, Anhui, China) supplemented with 10% fetal bovine serum (Biosharp, Anhui, China). All cell lines were maintained according to standard cell culture protocols.

Cytotoxicity Assay

To assess the cytotoxic effects of ALA (purity ≥98%, BD77466, CAS No.220620–09-7, Bidepharm, Shanghai, China) was used as provided by the manufacturer. No extraction process was performed as it was obtained from a commercial source. ALA was dissolved in DMSO.To eliminate solvent-specific effects, all treatment groups (0, 4, 8, and 16 μM ALA) received the same volume of DMSO, matching the concentration present in the 16 μM ALA group (final DMSO 0.0084%). Vehicle controls (0 μM ALA + 0.0084% DMSO) were included in all experiments.This concentration is 10-fold below the conventional cytotoxicity threshold (0.1%) for DMSO in cell cultures. Cytotoxicity assays were conducted on the six lymphoma cell lines and the Baf3 normal lymphocyte cell line using the Cell Counting Kit-8 (CCK-8; Boster, Wuhan, China). Cells were seeded at a density of $4x10^3$ cells/well in 96-well plates, and all cell lines were treated with ALA at concentrations of 0, 4, 8 and 16 μM for 48 h. After treatment, a mixture of 4 μL CCK-8 solution and 100 μL medium was added to each well, and incubated for 2 h. Absorbance was then measured at 450 nm using a Bio-Rad microplate reader (Bio-Rad, California, USA). The half maximal inhibitory concentration (IC50) values for each cell line

were calculated using GraphPad Prism (version 9,San Diego, CA, USA). Additionally, the Baf3 cell line was used to evaluate the cytotoxicity of ALA in normal cells.

Apoptosis Assay

Apoptosis was assessed by treating cells with varying concentrations of ALA (0, 4, 8 and 16 μM) for 48 h, followed by staining using the Annexin V-FITC Apoptosis Kit (Beyotime, Jiangsu, China) in accordance with the corresponding protocols. Detection was facilitated using the Becton Dickinson (BD) FACSCalibur flow cytometer (BD, USA), with subsequent analysis performed using FlowJo software (version10.8.1,Ashland, OR, USA).[24] Unstained, Annexin V single-stained, and PI single-stained samples were used to adjust voltages and set compensation parameters. During analysis, cell debris and doublets were excluded based on forward and side scatter (FSC/SSC) profiles. This assay was independently repeated three times.

Western Blotting (WB)

To assess the cytotoxic effects of ALA on human lymphoma cell lines, ALA was administered at concentrations of 0, 4, 8 and 16 μM for 48 h. Additionally, lymphoma cells harvested from mice with DEL treated with 0 and 5 mg/kg ALA were processed for protein extraction. According to the general WB protocols,[25] the expression levels of the following proteins were examined: β-tubulin, BCL2-associated X protein (Bax), BCL2, β-catenin, phosphorylated (p)-β-catenin (Ser675) (all from Cell Signaling Technology, Boston, USA), Caspase3, cellular Jun oncogene (cJun), glycogen synthase kinase 3β (GSK3β), p-GSK3β, Fas cell surface death receptor (Fas), Axis inhibition protein 1 (Axin1) and cyclin D1 (CCND1) (all from Abcam, San Francisco, USA). The assays used common WB reagents from Beyotime (Jiangsu, China), polyvinylidene fluoride membranes from Millipore (Massachusetts, USA) and an Enhanced Chemiluminescence Plus Assay Kit (dilution 1:1000) from Biosharp (Anhui, China). Analysis of band density was performed using ImageJ software (version 1.53t, National Institutes of Health, Bethesda, MD, USA).

Molecular Dynamics (MD) Simulation

In recent years, target screening of drugs has emerged as a focus of research, driven by analyses of interaction patterns and the binding free energy between receptors and ligands.[26] The present study conducted computational MD simulations to predict the mechanism of action of ALA. Autodock Vina software (version 1.1.2, Scripps Research, La Jolla, CA, USA) was used. The crystallographic structures of proteins utilized for screening and docking analyses were obtained from Protein Data Bank,[27] while the chemical structure of ALA was retrieved from the PubChem Substance and Compound databases.[28] The MD simulations of the docked ALA-protein complexes were conducted over 50 ns to determine their stability. The highest-scoring docking conformations were taken as the basis for subsequent MD calculations. The model outputs mainly included docking binding energy, the root mean square deviation (RMSD) value, the root mean square fluctuation (RMSF) value and the number of hydrogen bonds. Based on the trajectory data from MD simulations, the binding energies were quantified employing the Molecular Mechanics Generalized Born Surface Area approach.[29]

Cellular Thermal Shift Assay (CETSA)

Namalwa cells ($2 \times 10^{\wedge 6}$/mL) were treated with 32 μM ALA or DMSO (negative control) for 1 h at 37°C. Cells were harvested, aliquoted, and heated at 55–70°C for 3 min in PCR tubes. After cooling, cells were lysed by three freeze-thaw cycles in liquid nitrogen. Protein loading buffer was added, and lysates were analyzed by Western blotting to detect GSK3β and p-GSK3β. Melting curves were generated from the WB results to assess target stabilization.

Protein-Protein Interaction (PPI) Network Analysis

Based on the MD results, GSK3β emerged as a potential target, as it is a key regulator in the Wnt signaling pathway. To evaluate whether the Wnt signaling pathway mediates the inhibitory effects of ALA on DEL growth, the Search Tool for the Retrieval of Interacting Genes/Proteins (STRING) database was used to construct a PPI network of the targets.[30] Subsequently, PPI networks and related information were employed to generate the GSK3β network model via

Cytoscape (version 3.9.0, San Diego, CA, USA). Additionally, the potential proteins and related genes affected by ALA were analyzed.

Gene Set Variation Analysis (GSVA)

GSVA was performed to explore enriched pathways in patients with DEL using the GSVA package (version 1.36.2, Bioconductor, http://bioconductor.org).[31] Gene sets were downloaded from the Molecular Signatures Database, and differences in pathway activity scores per sample were calculated using the *t*-test.

Gene Ontology (GO) Enrichment Analysis

Data (accession no. GSE85446) from MC38 tumor tissues treated with ALA and iso-ALA were selected from the Gene Expression Omnibus database. DESeq2 and GO analysis were used to explore different genes and enrichment pathways between the vehicle and ALA groups based on R package (R Foundation for Statistical Computing, https://www.R-project.org/), and were visualized with GO package (version 4.3.2, Bioconductor, http://bioconductor.org) ($P \leq 0.05$).[32]

Cell Immunofluorescence Assay

To ascertain the subcellular localization of GSK3β and β-catenin, immunofluorescence staining was employed. Namalwa cells, in logarithmic growth phase (1.5x106/well), were treated with 8 μM ALA for 48 h in 6-well plates, with DMSO serving as the control group. The cells were then fixed with methanol for 8 min and vortexed for resuspension. After permeabilization with 0.1% Triton X-100, the samples were blocked with a mixture of 1% BSA (Bovine Serum Albumin, Merck, Darmstadt, Germany) and 0.1% Triton X-100. Primary antibodies against β-catenin and GSK3β (dilution 1:200) were then incubated with the cells overnight. The samples were incubated with FITC-labeled Goat Anti-Rabbit IgG (dilution 1:200) in the dark for 2 h on the 2nd day. Subsequently, the cells were stained with DAPI (Boster, Wuhan, China) for 10 min and images of the cells were captured using a confocal laser scanning microscope (TS100-F; Nikon, Japan) at a magnification of x100.

Expression of Wnt Target Genes and Apoptosis-Related Genes

Six human lymphoma cell lines were assessed by reverse transcription-quantitative PCR (RT-qPCR) to determine the expression levels of BCL2. Total ribonucleic acid (RNA) was extracted utilizing Trizol reagent (Boster, Wuhan, China) according to the manufacturer's protocol, and 1,000 ng total RNA was used for RT to generate cDNA using a RT kit (Beyotime, Jiangsu, China). The product of cDNA synthesis was then amplified using the Fast SYBR Green Quantitative Polymerase Chain Reaction (qPCR) Master Mix Kit (Rongwei, Chengdu, China). The primer sequences for BCL2 were as follows:[33] Forward, CTGTGGATGACTGAGTACC; reverse, CAGCCAGGAGAAATCAAAC. The primer sequences for β-tublin:[34] Forward:ctggcaccatggactctg Reverse:tcggctccctctgtgtag

Histological Analysis

For hematoxylin and eosin (H&E) staining, cervical lymph node tissues from mice in the DEL and control groups were fixed overnight in 4% paraformaldehyde (Beyotime, Jiangsu, China). The tissues were then embedded in paraffin and sliced into 6-μm sections, which were stained with H&E (Kohypath, Shanghai, China) according to the protocol of the manufacturer. Hematoxylin stained the nuclei blue and eosin stained the cytoplasm. Images of the sealed slides were captured using a stereomicroscope to observe pathological changes at a magnification of X20.

Two-Photon Excitation Fluorescence Imaging

Initially, the cervical lymph nodes from mice with DEL were fixed using paraformaldehyde. The tissues were then immobilized on a transparent glass dish overnight using glycerol gelatin (Beyotime, Jiangsu, China). Subsequently, the specimen was placed in the operational chamber of an Olympus MPE-*RS* two-photon excitation microscope (Olympus Corporation, Tokyo, Japan). Wavelengths of 780 nm for green fluorescence and 1,100 nm for red fluorescence were selected to excite fluorescence. One-dimensional photographs or three-dimensional stereo images were captured, based on the red or green fluorescence signals.

Primary DEL Mouse Model

Male C57BL mice (age, 6 weeks; weight, ~20 g) were purchased from the Chinese Academy of Sciences (Shanghai, China). The experimental mice were irradiated with 3.5 Gy X-ray to destroy the bone marrow, and 1,000,000 CD19+ pre-B cells from bone marrow of wild-type mice were co-infected with a retrovirus encoding BCL2 and cellular myelocytomatosis oncogene (cMyc), and were transplanted into sub-lethally irradiated C57BL mice by tail vein injection. The mice were monitored weekly and lymphoma development was observed in the mice within 3 weeks. Tumors were checked every other day; in the mice, the largest tumor volume detected was 48 mm3, the longest diameter was 6 mm and the longest width was 4 mm.

The mice with lymphoma were randomly divided into two groups (n = 6 per group). The sample size was determined based on preliminary experiments showing low intra-group variability and was consistent with previous MYC/BCL2-driven lymphoma studies.[35] Vehicle and ALA, and underwent treatment for 10 days. ALA was administered at a concentration of 5 mg/kg. Fluorine-18 fluorodeoxyglucose (18F-FDG) was administered to mice via intraperitoneal injection, and 18F-FDG positron emission tomography-computed tomography (PET-CT) (General Electric Company, Boston, USA) was used to detect lymphoma by fluorescence signal intensity before and after treatment. The mice were continuously bred to assess survival outcomes. The tumor volumes were measured by a trained technician in PET imaging. If the mice survived until the end of the experiment, the mice were euthanized via CO2 asphyxiation, and lymph tissues were collected for HE and WB analyses.

Statistical Analysis

Statistical analyses were performed using GraphPad Prism (version 9, https://www.graphpad.com). Continuous variables were presented as the mean or median. One-way analysis of variance (ANOVA) was used to compare multiple groups, and planned comparisons between the experimental and control groups were made using Dunnett's post hoc test if statistically significant differences were found by ANOVA. The Kaplan-Meier method was used to assess the survival rates of patients with DEL, and mice with DEL treated with either the vehicle or ALA. $P<0.05$ was considered to indicate a statistically significant difference, whereas $P<0.01$ was considered highly significant. The results were substantiated by sufficient biological and technical replicates ($n\geq3$).

Results

Correlation Between Wnt-β-Catenin Signaling Pathway and DEL

To elucidate the molecular mechanisms underlying dual-expression lymphoma (DEL), we employed Gene Set Variation Analysis (GSVA) to analyze pathways in patients with DEL. The GSVA findings revealed a positive correlation between the Wnt/β-catenin signaling pathway and DEL. Conversely, the negative regulation of the Wnt signaling pathway exhibited inverse associations with DEL (Figure 1A). Furthermore, the STRING database was utilized to construct a protein-protein interaction (PPI) network to explore the underlying mechanisms. The results showed that GSK3B is also centrally located within the network, interacting with multiple proteins, indicating its potential significant role in the disease. GSK3β, a crucial molecule for the degradation of β-catenin in the Wnt signaling pathway, was demonstrated in the PPI analysis (Figure 1B).

Molecular Docking of ALA and Its Interaction Network with the Wnt Pathway

Based on STRING database analysis (Cytoscape 3.90), ALA was predicted to target proteins and genes associated with the Wnt-protein binding pathway and negative regulation of the non-canonical Wnt signaling pathway (Figure 2A). Given the central role of GSK3β in the Wnt/β-catenin cascade where it phosphorylates β-catenin for proteasomal degradation[023],we hypothesized that pharmacological inhibition of GSK3β could disrupt oncogenic Wnt activation in lymphoma.Molecular docking demonstrated that ALA binds to the ATP pocket of GSK3β, forming: Hydrogen bonds with LEU-132 and ASP-200;Hydrophobic interactions with LEU-188 and ILE-62 (Figure 2B).The ALA-GSK3β complex (red line) exhibited greater stability (RMSD: 2.5–3 Å) than apo-GSK3β (black line; RMSD: 1.5–2.5 Å) (Figure 2C).RMSF analysis revealed reduced flexibility in residues 200–215, suggesting ALA-induced

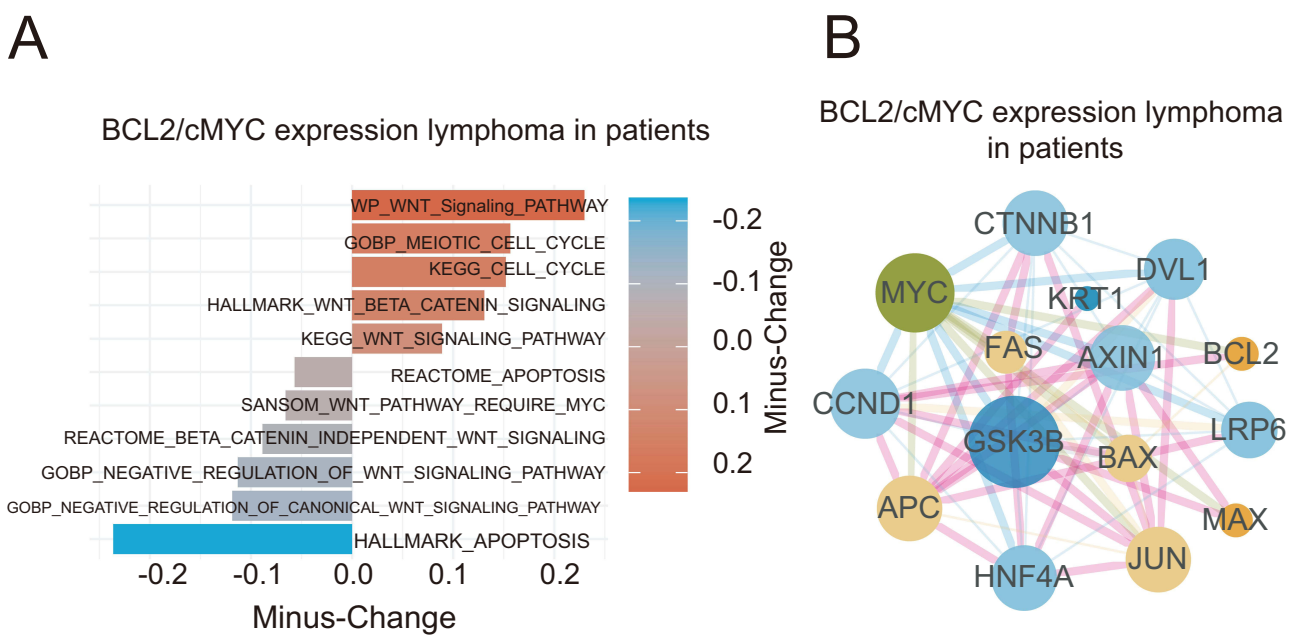

Figure 1 WNT Pathway and GSK3β-Centered Network Dysregulation in DEL (**A**) GSVA image depicting enrichment analysis of the Wnt signaling pathway in patients with DEL. (**B**) Nodes represent individual proteins, with larger nodes indicating key proteins in PPI network diagram. The result indicates that the key genes GSK3β and Axin1 in the Wnt pathway are enriched.
Abbreviation: GSVA, Gene Set Variation Analysis.

conformational stabilization (Figure 2D).The binding energy (−15.66 ± 2.15 kcal/mol) indicated strong affinity (Figure 2E).Moreover, CETSA Validates Target Engagement Consistent with docking predictions, CETSA confirmed ALA-mediated stabilization of GSK3β:GSK3β melting temperature (Tm) increased in ALA-treated samples (stable up to 70°C vs control Tm: 61°C).Phospho-GSK3β (p-GSK3β) in ALA-treated groups showed delayed degradation (control: complete degradation at 67°C) (Figure 2F–I).These results establish GSK3β as a critical pharmacological target of ALA, with mechanistic insights into its allosteric stabilization and potential to modulate Wnt-driven oncogenesis.

ALA Alleviates DEL in vitro and in vivo

To determine whether ALA suppresses lymphoma growth in vitro, a CCK-8 assay was performed to evaluate its anti-lymphoma activity in human lymphoma cell lines. The results showed that ALA exhibited dose-dependent cytotoxicity across all tested cell lines (Figure 3A). The IC50 values of ALA in the six cell lines, ranked from high to low, were as follows: Ramos, Raji (10.97 μM), Namalwa (6.23 μM), SUDHL-6, SUDHL-4, and Kasumi. Except for Ramos cells, the IC50 values in all other cell lines were below 11 μM, with four close to 6 μM. A schematic diagram of the animal experimental design is shown in Figure 3B. PET-CT imaging was employed to monitor DEL-bearing mice before and after treatment. As depicted in the PET-CT images, lymphomas in ALA-treated mice were effectively suppressed, whereas those in vehicle-treated mice exhibited progressive enlargement (Figure 3C). As shown in Figure 3D, tumor volume in the cervical region increased in the control mice but decreased in ALA-treated mice, as indicated by the white arrows. Correspondingly, the mean standardized uptake value (SUV) of tumor lesions was significantly lower in the ALA-treated group than in the vehicle group, which showed a marked increase ($P < 0.01$ vs control; Figure 3E). Moreover, Kaplan–Meier survival analysis revealed that the median survival time of vehicle-treated mice with DEL was 50 days, whereas ALA-treated mice survived up to 80 days, indicating a significantly prolonged survival ($P < 0.05$ vs control; Figure 3F). Representative H&E-stained sections of cervical lymph nodes from control and ALA-treated mice

https://doi.org/10.2147/BLCTT.S556751

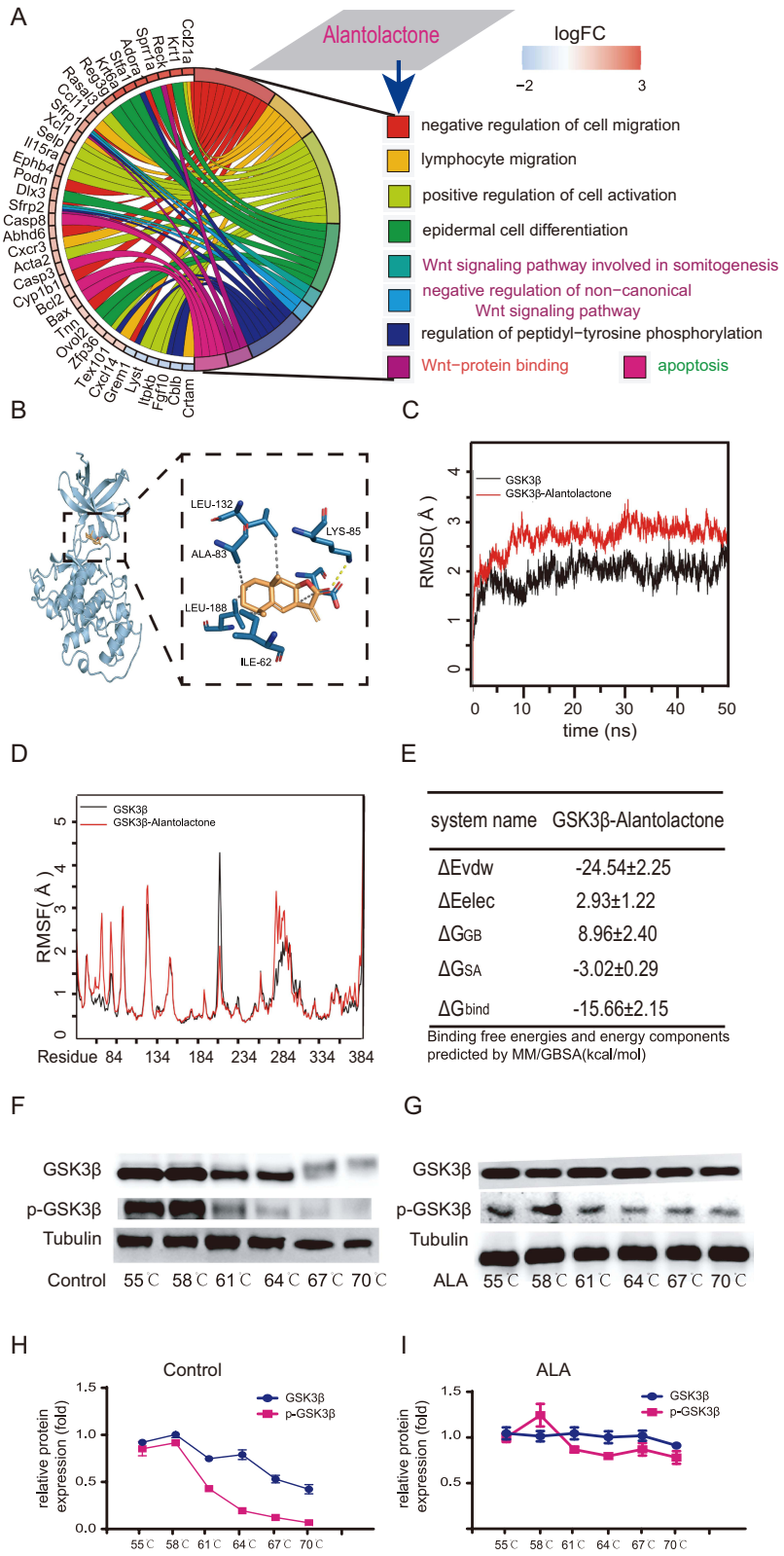

Figure 2 Results of molecular dynamics simulation and CETSA for GSK3β. (**A**) GO enrichment analysis, presented as a chord diagram. (**B**) Molecular docking diagram showing the interaction between ALA and GSK3β. (**C**) RMSD, (**D**) RMSF, (**E**) binding energy of ALA with GSK3β. (**F**) Protein obtained from CETSA followed by detection with WB (**G**). Melting curves were calculated based on WB quantification analysis (**H** and **I**).

Abbreviations: CETSA, Cellular thermal shift assay; RMSD, root mean square deviation; RMSF, root mean square fluctuation; Δevdw, van der Waals energy; ΔEelec, electrostatic energy; ΔGGB, electrostatic contribution to solvation; ΔGSA, non-polar contribution to solvation; ΔGbind, binding free energy.

https://doi.org/10.2147/BLCTT.S556751

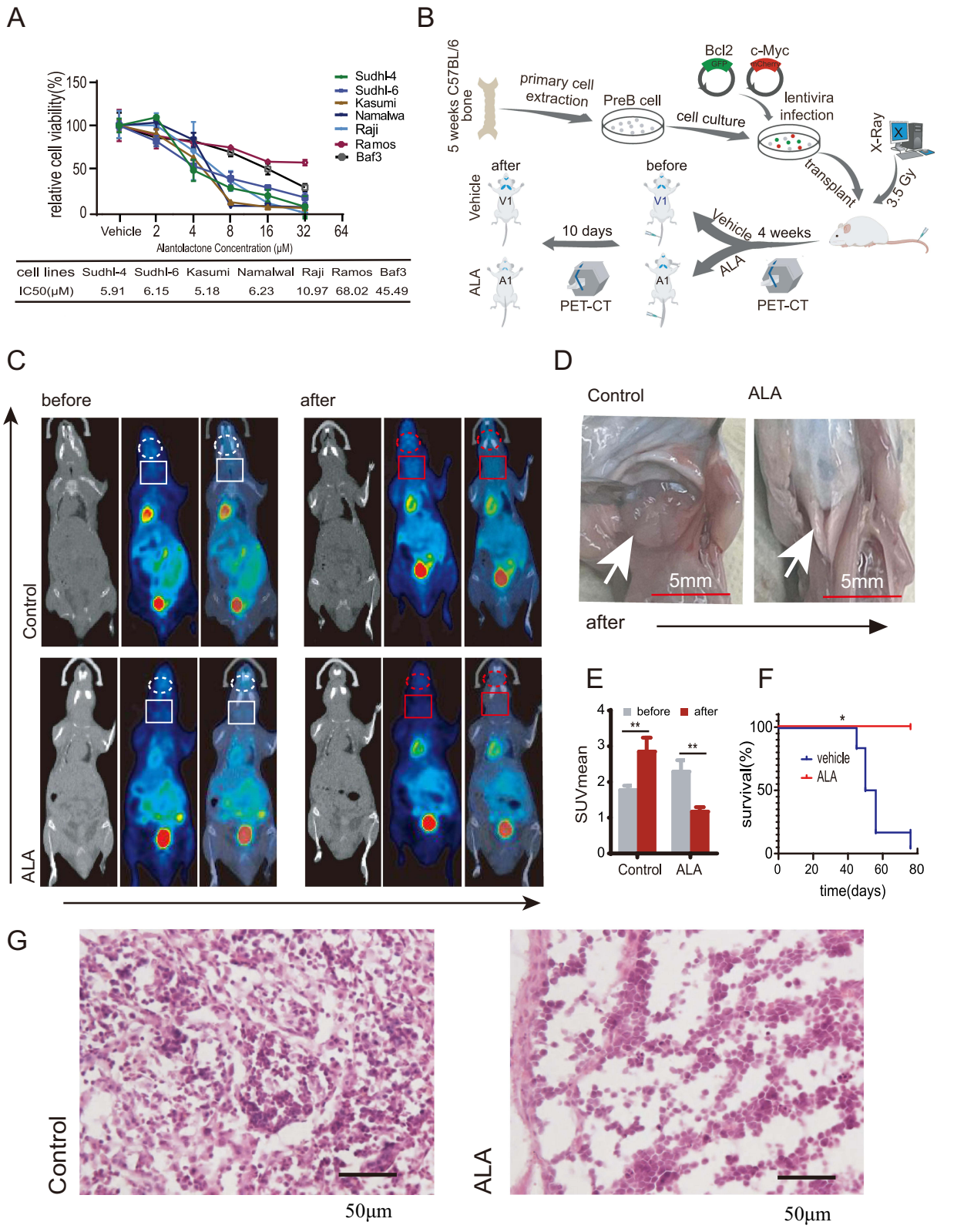

Figure 3 ALA inhibits lymphoma growth in DEL C57BL mice.(**A**) Cytotoxicity of ALA against six lymphoma cell lines, with IC_{50} values presented.(**B**) Schematic diagram of the DEL mouse model.(**C**) PET-CT images showing reduced tumor volume in ALA-treated mice compared with control mice (highlighted by circles or boxes).(**D**) Cervical tumor volume increased in control mice but decreased in ALA-treated mice.(**E**) Comparison of SUVmean before and after ALA treatment, showing a marked reduction.**P < 0.01 compared with before treatment.(**F**) Kaplan–Meier survival curves of ALA-treated versus control mice.*P < 0.05, compared with control.(**G**) Representative H&E staining of cervical lymph nodes (40× magnification); black arrows indicate DEL cells.

Abbreviations: DEL, dual-expression lymphoma; ALA, alantolactone.

https://doi.org/10.2147/BLCTT.S556751

are shown at 40× magnification (Figure 3G). Collectively, these findings demonstrate that ALA effectively inhibits DEL growth in vivo.

The Wnt Signaling Pathway as a Potential Pharmacological Mechanism of ALA in Inhibiting Lymphoma

To assess the impact of GSK3β enrichment on DEL outcomes, survival analysis was performed to compare the difference between patients with DEL exhibiting high and low GSK3β expression. As shown in Figure 4A, patients with DEL exhibiting high GSK3β expression had significantly better overall survival compared with those with low expression.To further explore the mechanism of GSK3β acting on ALA, Cellular immunofluorescence staining was employed to ascertain the localization of p-GSK3β and β-catenin in lymphoma cells treated with or without ALA. In the ALA-treated group, increased cytoplasmic accumulation of p-GSK3β and decreased nuclear localization of β-catenin were observed compared with the control group at ×40 magnification (Figure 4B). These results indicate that ALA enhances p-GSK3β phosphorylation, thereby preventing β-catenin translocation into the nucleus.This result verified that ALA can increase p-GSK3β to prevent β-catenin translocation into nucleus. To determine whether the levels of protein associated with the Wnt signaling pathway were affected by ALA, WB was carried out forNamalwa cell line (Figure 4C). The expression levels of Axin1 and p-GSK3β were significantly upregulated at the protein level in a dose-dependent manner, whereas total GSK3β protein levels remained unchanged (Figure 4D–F). P-β-catenin (Ser675) induces β-catenin accumulation and transcriptional activity in the nucleus.[15] The present study chose p-β-catenin (Ser675) to detect the effects of ALA on nuclear β-catenin accumulation. As shown in Figure 4G and H, the expression levels of total β-catenin and p-β-catenin (Ser675) in Namalwa cells was decreased with an increasing concentration of ALA ($P<0.05$). An investigation into the effective mechanism of ALA was also performed on Raji cells, another human lymphoma cell line, and similar results were observed (Figure 4I–K). We also examined changes in Wnt-related proteins in mice with DEL. As shown in Figure 4L, the expression levels of p-GSK3β and Axin1 were significantly increased compared with those in the vehicle group, whereas the protein expression of total GSK3β was markedly decreased. Total β-catenin and p-β-catenin (Ser675) were decreased in DEL cells ($n=3$, $P<0.05$).Collectively, these findings suggested that inhibition of the Wnt signaling pathway may constitute a pharmacological mechanism through which ALA exerts its anticancer effects.

ALA Binds Closely to the BCL2 Protein to Change its Conformation, Which in Turn Inhibits its Function in Apoptosis

At the same time, ALA may regulate apoptosis-related genes, which are mainly linked to apoptotic genes and corresponding proteins based on the PPI network analysis (Figure 5A and B). According to the prediction of ALA-binding targets, BCL2 emerged as one of the top binding candidates of ALA. MD simulations were subsequently utilized to analyze the binding conformation of the ALA-BCL2 complex, and the results indicated that ALA binds to the internal cavity of the BCL2 protein. As shown in Figure 5C, ALA formed hydrophobic interactions with ALA-149, methionine-115, phenylalanine-112, LEU-137 and valine-133 on the BCL2 protein to stabilize the ALA-BCL2 complex, indicating that formation of the ALA-BCL2 complex could affect the biological functions of BCL2. The RMSD from MD simulations reflects the motion trajectory of the complex, with greater RMSD fluctuations indicating more pronounced motion and vice versa. Notably, the RMSD of the complex exceeded that of unbound BCL2 (Figure 5D), suggesting that ALA binding induced conformational and dynamic changes in BCL2, potentially leading to a loss of its original physiological functions.RMSF can reflect the flexibility of the protein during MD simulation. Usually, the changes in protein flexibility can exert the enzyme-activating effect in drug-target interactions. As shown in Figure 5E, the black line indicated the RMSF without binding, and the red line indicated the RMSF of the complex. The overall RMSF of the complex increased, which suggested that ALA could influence the flexibility of BCL2, and further affect its stability and dynamically alter its conformation to exert a biological effect. The binding energy between ALA and BCL2 was calculated to be −22.22±2.16 kcal/mol (Figure 5F). Lower values indicate stronger binding; therefore, −22.22 kcal/mol indicates a strong binding affinity between BCL2 and ALA. Furthermore, as shown in Figure 5G and H, the results of CETSA demonstrated that after ALA treatment, BCL2 expression remained stable even at 70°C, whereas BCL2 melted

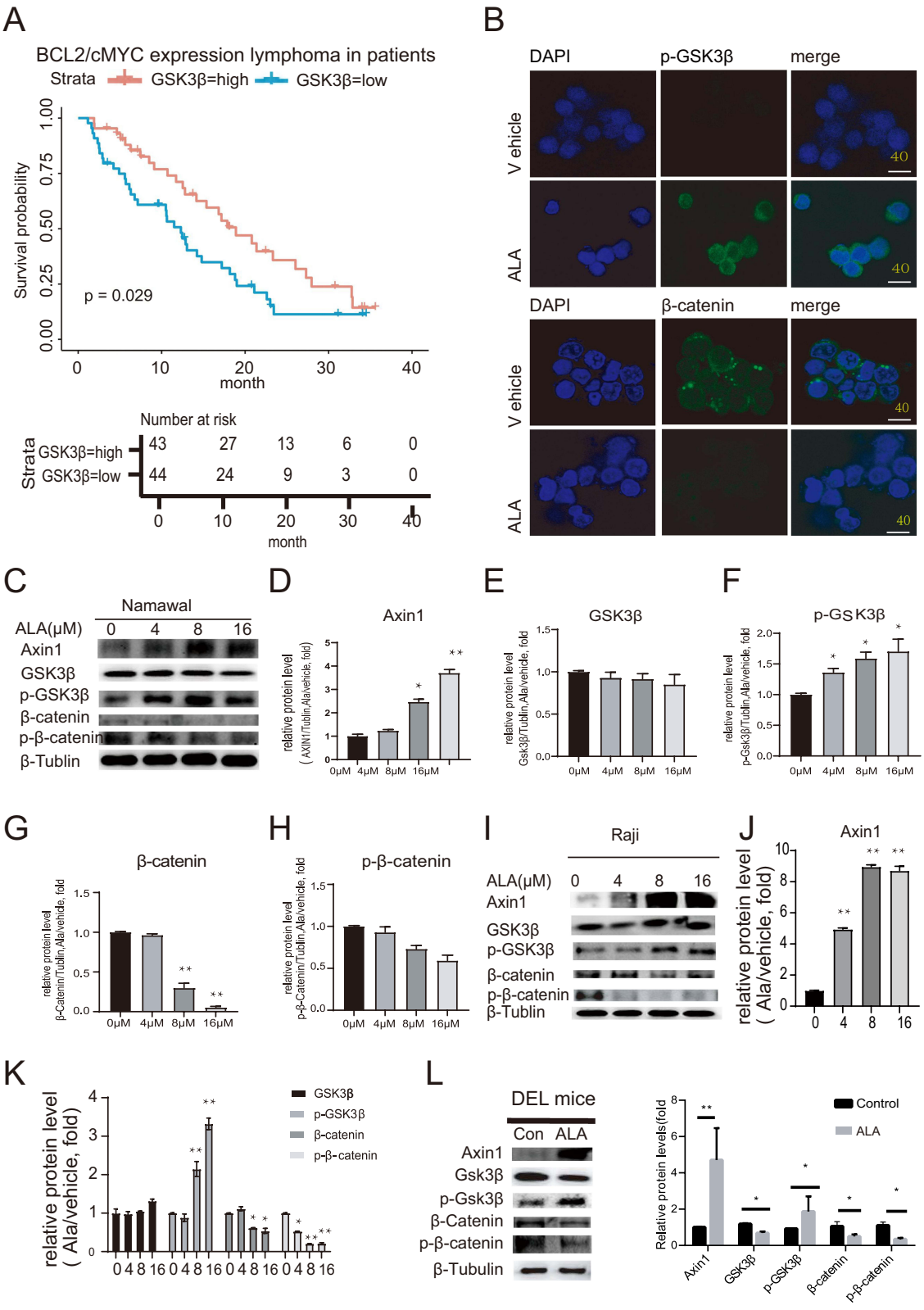

Figure 4 ALA exerts its therapeutic effect by promoting the degradation of key proteins in the Wnt-related pathway. (**A**) Comparison of survival analysis between patients with DEL and DLBCL. (**B**) Representative images of immunofluorescence staining showing the localization of p-GSK3β and β-catenin (×100 magnification; scale bar=50 μm). Blue indicates location of the nucleus (DAPI), and green represents GSK3β or β-catenin. (**C**) Wnt pathway-related protein expression, including Axin1, GSK3β, p-GSK3β, β-catenin and p-β-catenin in Namalwa cells using WB.(**D**–**H**) Quantitative grayscale analysis of protein expression in Namalwa cells: (**D**) Axin1, (**E**) GSK3β, (**F**) p-GSK3β, (**G**) β-catenin, (**H**) p-β-catenin. (**I**–**K**) Raji cell analysis: (**I**) Representative images of Wnt pathway-related protein expression (**K**) Quantitative grayscale analysis for GSK3β, p-GSK3β, β-catenin and p-β-catenin levels (n=3). (**L**) In vivo validation in DEL mouse models: Western blot and semi-quantitative analysis of Wnt pathway proteins (Axin1, GSK3β, p-GSK3β, β-catenin, and p-β-catenin). Data are presented as mean ± SD (n = 3); *P < 0.05, **P < 0.01 compared with control.

https://doi.org/10.2147/BLCTT.S556751

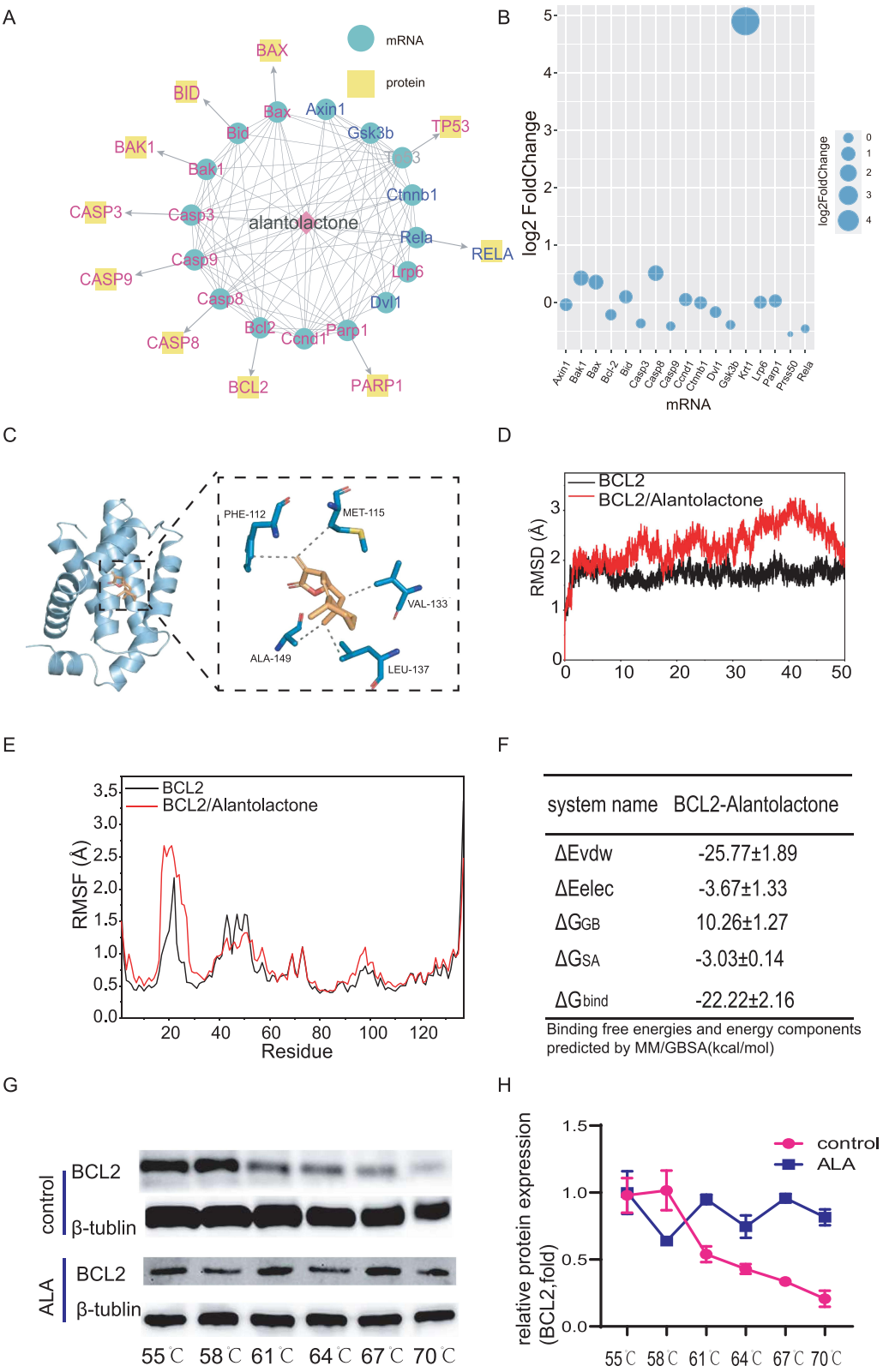

Figure 5 Results of molecular dynamics simulation and CETSA for BCL2.(**A**) Network diagram of drug-target protein interactions with ALA in the center. Yellow represents the possible proteins which ALA acted on, blue represents the possible target genes, and pink represents apoptosis-related proteins or genes. (**B**) Bubble plot showing the alterations of genetic levels in lymphoma cells after ALA treatment. The sizes of the bubbles indicate the gene expression levels.(**C**) Molecular docking diagram illustrating the interaction between ALA and its target, BCL2. (**D**) RMSD, (**E**) RMSF (**F**) binding energy calculation for ALA and BCL2 interaction. (**G**) WB analysis of BCL2 protein levels based on CETSA. (**H**) Melting curves were calculated based on WB results.

Abbreviations: CETSA, Cellular thermal shift assay; RMSD, root mean square deviation; RMSF, root mean square fluctuation.

https://doi.org/10.2147/BLCTT.S556751

in the control group at 61°C. These findings highlight BCL2 as a critical target site of ALA performing pharmacological effects, enhancing its thermal stability and impacting its biological function.

ALA Induces Apoptosis in vitro and in vivo

To explore whether ALA suppresses induces apoptosis in vitro, we tested the mRNA levels of the anti-apoptotic protein BCL2 in several human lymphoma cell lines as shown in Figure 6A, the mRNA levels of BCL2 in decreasing order, were Kasumi, SUDHL-6, SUDHL-4,Namalwa, Raji and Romas. To determine the ability of ALA to induce apoptosis, an apoptotic assay was performed onNamalwa and Raji cell lines. As shown in Figure 6B, ALA induced apoptosis inNamalwa cells in a concentration-dependent manner ($P<0.01$). To further observe the anti-apoptotic effect of ALA, changes in the proteins related to cell apoptosis and proliferation were detected inNamalwa cells after treatment with 0, 4, 8 and 16 μM ALA for 48 h. Compared to the control, In the ALA-treated group, the mitochondrial-dependent apoptotic proteins Bax and Caspase3 were increased, but BCL2 levels were significantly decreased in a concentration-dependent manner (Figure 6C). In addition, the expression of essential genes in the extrinsic apoptotic pathway, Fas and cJun, were detected. The expression of Fas was obviously increased, whereas the levels of cJun were decreased by ALA in a dose-dependent manner. Furthermore, the protein levels of oncogene and cell cycle-related genes, including cMyc and CCND1, were all decreased by ALA (Figure 6D). Similar results were observed in Raji cells, as shown in Figure 6E–G. These results suggested that ALA treatment may induce apoptosis. Furthermore, WB analysis was performed in vivo to verify the prediction. As shown in Figure 6H, compared with in the control group, ALA caused a significant upregulation of Bax and Caspase3, and a downregulation of BCL2, indicating that ALA induced the mitochondrial-mediated apoptosis pathway in mice with DEL. Additionally, Fas, a protein related to the extrinsic apoptotic pathway, was markedly upregulated (Figure 6I). Additionally, two-photon excitation fluorescence imaging was performed to assess the changes in BCL2- and cMyc-positive lymphoma cells between the control and ALA-treated mice. As shown in Figure 6J, compared with in the control group, cMyc- and BCL2-positive lymphoma cells were markedly decreased in ALA-treated mice.

Discussion

Standard R-CHOP therapy is less effective in treating DEL, which is prone to relapse and exhibits chemotherapy resistance. The present study demonstrates that ALA exhibits significant anti-tumor activity in DEL by modulating the Wnt/β-catenin signaling pathway and inducing apoptosis. Our findings suggest that ALA may serve as a promising natural compound for DEL treatment, with a dual mechanism involving GSK3β inhibition and BCL2 suppression. GSK3β is a key molecule in the Wnt pathway,The ALA-induced cytoplasmic retention of p-GSK3β likely prevents β-catenin nuclear translocation, a critical step in Wnt-driven oncogenesis verified by confocal laser scanning microscope and Western blot.There are several Wnt/β-catenin modulators that have been used in clinical trials and showed promising results, such as in medulloblastoma (NCT01878617), triple-negative breast cancer (NCT01351103) and gastrointestinal cancer (NCT03355066).[17,36,37] ALA maybe a potential drug for DEL.

Network pharmacology predictions and MD studies demonstrated that ALA can bind to the ATP pocket of GSK3β and the BCL2 hydrophobic pocket. This structural perturbation may explain the observed Bax/Caspase3 activation and synergize with Wnt inhibition to enhance tumor cell death. CETSA further confirmed that ALA can stabilize GSK3β and BCL2, In vivo, PET - CT imaging and tumor volume measurements demonstrated that ALA effectively suppressed lymphoma growth in mice with DEL. The Kaplan - Meier curves also revealed a significantly longer survival time in ALA - treated mice compared to the control group. These results strongly suggest that ALA has the potential to be a therapeutic agent for DEL.In addition, ALA exhibited low toxicity to normal cells in DEL mice.

Conclusion

This study establishes ALA as a first-in-class natural compound that exerts potent anti-tumor activity in DEL involving GSK3β inhibition preventing β-catenin nuclear translocation and directly binding to BCL2 to overcome apoptotic resistance. While our findings are promising, they must be contextualized within the current therapeutic landscape for DEL. The recent success of the HDAC inhibitor chidamide in the DEL study validates the strategy of indirect MYC inhibition,[38] while the failure of venetoclax combined with R-CHOP underscores the challenge of singularly targeting the

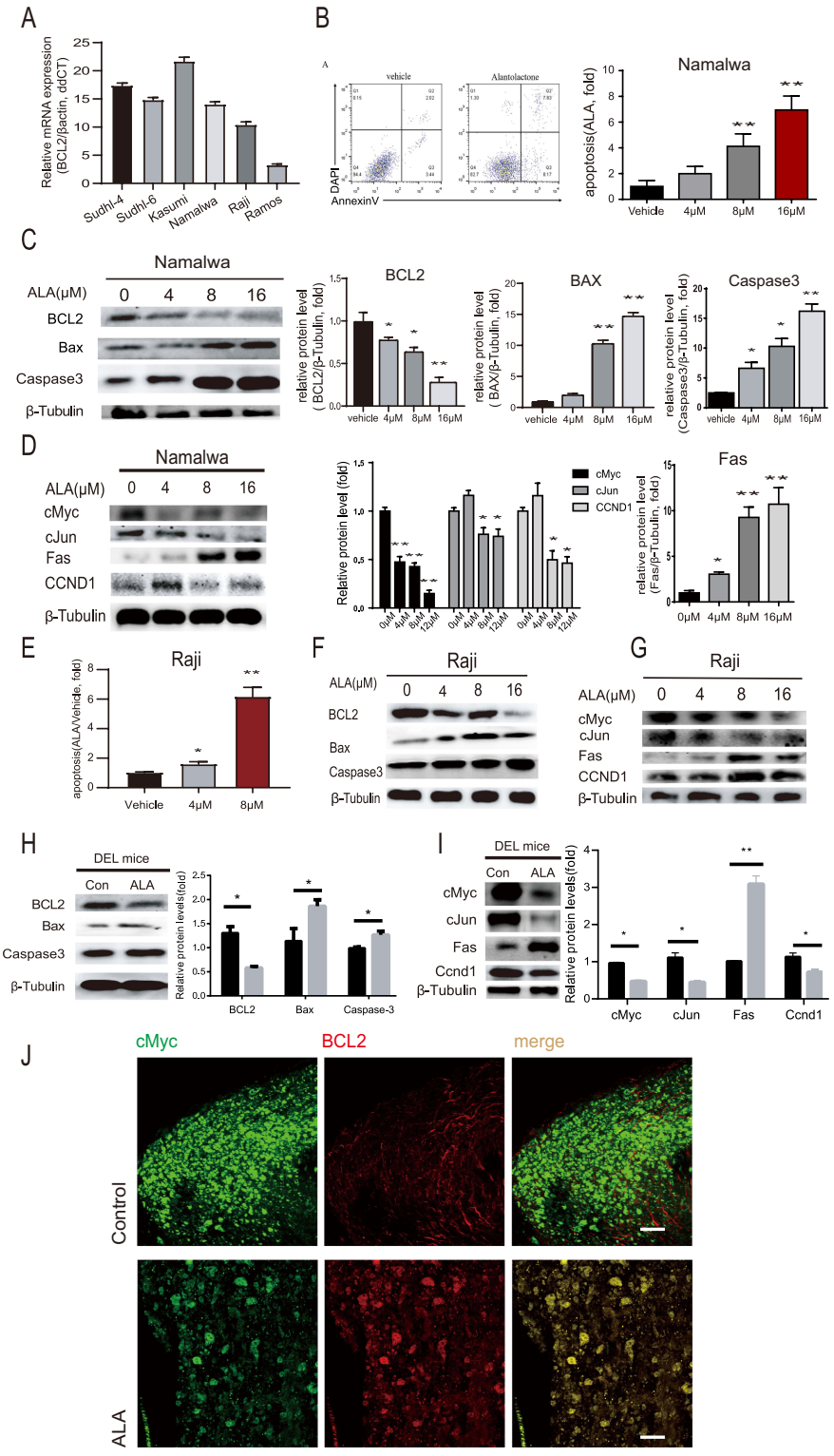

Figure 6 ALA inhibits proliferation and induces apoptosis in human lymphoma cell lines. (**A**) BCL2 mRNA expression profile across six lymphoma cell lines. (**B**)Flow cytometric analysis showing ALA induced the apoptosis ofNamalwa cells. (**C**) Dose-dependent modulation of apoptosis-related proteins (BCL2, Bax, Caspase3) in Namalwa cells with WB.(**D**) Representative images and protein expression levels showing the changes in cMyc, cJun, Fas and CCND1 expression levels in Namalwa cells treated with 0, 4, 8 and 16 μM ALA for 48 h. (**E**) Flow cytometric analysis demonstrating ALA-induced apoptosis in Raji cells treated with 0, 4, and 8 μM ALA for 48 h. (**F**) Representative Western blot images showing alterations in BCL2, Bax, and Caspase3 protein levels in Raji cells.(**G**) Representative images showing alterations in cMyc, cJun, Fas, and CCND1 expression in Raji cells.(**H**) Western blot analysis and quantification of BCL2, Bax, and Caspase3 expression in DEL mice.(**I**) Representative images and quantitative analysis showing the changes in cMyc, cJun, Fas, and CCND1 protein levels in DEL mice. Tubulin served as a loading control. Comparisons were made between ALA-treated and vehicle-treated groups.Data are presented as the mean ± SD (n = 3). *P < 0.05, **P < 0.01 vs control.(**J**) Two-photon fluorescence imaging of cMyc (green) and BCL2 (red) co-localization.

BCL2 axis.[39] Our work positions ALA as a unique agent capable of concurrently addressing both of these core vulnerabilities, offering a mechanistically distinct approach.

Additionally, ALA exerts pleiotropic effects by modulating additional signaling pathways, including ROS generation, AKT activity, and STAT3 signaling, which may contribute to its overall therapeutic efficacy.[19,23] These multifaceted actions underscore the complexity of ALA's biological impact and warrant deeper mechanistic investigation.

However, several critical questions must be addressed to advance this work. First, given that most novel agents achieve their greatest clinical impact in rational combinations, future work should prioritize evaluating ALA in combination with standard therapies (eg, R-CHOP) as well as with other targeted agents. Second, the translational path for ALA requires solving key pharmaceutical challenges, notably its aqueous solubility, through advanced drug delivery strategies and comprehensive pharmacokinetic and safety assessments. In conclusion, by delineating a novel dual-targeting mechanism, our study establishes ALA not just as a candidate but as a foundational framework for building more effective, combination-based strategies to overcome therapeutic resistance in DEL.

Ethics Statement

All animal experiments were performed in accordance with the Guidelines for the Care and Use of Laboratory Animals and were approved by the Animal Ethics Committee of North Sichuan Medical College (approval No:2022-031).

The use of gifted cell lines in this study was reviewed and approved by the Institutional Research Ethics Committee of North Sichuan Medical College (approval No:2025-037), in accordance with institutional and journal ethical requirements.The TCGA datasets in this study are publicly available and de-identified human data, and thus exempt from ethics review per Article 32 (Items 1 and 2) of the Measures for Ethical Review of Life Science and Medical Research Involving Human Subjects (effective 18 February 2023).

Acknowledgments

We would like to thank Professor Chong Chen from the State Key Laboratory of Sichuan University for the generous gift of human lymphoma cell lines (Kasumi, Namalwa, SUDHL-4, SUDHL-6, Raji, Ramos) and the normal B lymphocyte cell line Baf3 (mouse).

Financial support: This work was supported by the Project of the Bureau of Science & Technology Nanchong City (19SXHZ0303, 19SXHZ0443), Project for the First-class Pharmaceutical Sciences of North Sichuan Medical College (CYB21-YLXK03), Project for Affiliated Hospital of North Sichuan Medical College (2020ZD004).

Project for Xi Jinping Thought on Socialism with Chinese Characteristics for a New Era (2024YB001).

Disclosure

The authors declare no conflicts of interest.

References

1. Bray F, Laversanne M, Sung H, et al. Global cancer statistics 2022: GLOBOCAN estimates of incidence and mortality worldwide for 36 cancers in 185 countries. *CA Cancer J Clin*. 2024;74(3):229–263. doi:10.3322/caac.21834
2. Shi Y. Current status and progress of lymphoma management in China. *Int J Hematol*. 2018;107(4):405–412. doi:10.1007/s12185-018-2404-8
3. Chen SY, Xu PP, Feng R, et al. Extranodal diffuse large B-cell lymphoma: clinical and molecular insights with survival outcomes from the multicenter EXPECT study. *Cancer Commun*. 2025;45(8):919–935. doi:10.1002/cac2.70033
4. Song X, Rao H, Guo C, et al. Myricetin exhibits selective anti-lymphoma activity by targeting BTK and is effective via oral administration in vivo. *Phytomedicine*. 2021;93:153802. doi:10.1016/j.phymed.2021.153802
5. Swerdlow SH, Campo E, Pileri SA, et al. The 2016 revision of the world health organization classification of lymphoid neoplasms. *Blood*. 2016;127:2375–2390. doi:10.1182/blood-2016-01-643569
6. Zhang M, Wu Y, Cheng Z, et al. Zanubrutinib plus R-CHOP improves the treatment effect of newly diagnosed diffuse large B cell lymphoma with double expression of MYC and BCL-2. *Front Immunol*. 2025;16:1526318. doi:10.3389/fimmu.2025.1526318
7. Yin Y. DEL variants: review of molecular mechanisms, clinical consequences and molecular testing strategy. *Funct Integr Genomics*. 2023;23:318. doi:10.1007/s10142-023-01249-z
8. Karmali R, Shouse G, Torka P, et al. Double hit & double expressor lymphomas: a multicenter analysis of survival outcomes with CD19-directed CAR T-cell therapy. *Blood Cancer J*. 2025;15(1):43. doi:10.1038/s41408-025-01250-8
9. Kobold S, Müller R. Aktuelle fortschritte und neue therapieoptionen in der immunonkologie [Current progress and latest therapeutic options in immuno-oncology]. *Dtsch Med Wochenschr*. 2025;150(22):1335–1340. doi:10.1055/a-2502-1305

10. Herrera AF, Mei M, Low L, et al. Relapsed or refractory double-expressor and double-hit lymphomas have inferior progression-free survival after autologous stem-cell transplantation. *J Clin Oncol*. 2017;35(1):24–31. doi:10.1200/JCO.2016.68.2740
11. Jiang J, Wang J, Yue M, Liu H, et al. Direct phosphorylation and stabilization of MYC by aurora B kinase promote T-cell leukemogenesis. *Cancer Cell*. 2020;37(2):200–215.e5. doi:10.1016/j.ccell.2020.01.001
12. Prochownik EV, Vogt PK. Therapeutic targeting of Myc. *Genes Cancer*. 2010;1(6):650–659. doi:10.1177/1947601910377494
13. Domoto T, Uehara M, Bolidong D, et al. Glycogen synthase kinase 3β in cancer biology and treatment. *Cells*. 2020;9(6):1388. doi:10.3390/cells9061388
14. Murakami K, Terakado Y, Saito K, et al. A genome-scale CRISPR screen reveals factors regulating Wnt-dependent renewal of mouse gastric epithelial cells. *Proc Natl Acad Sci USA*. 2021;118(4):e2016806118. doi:10.1073/pnas.2016806118
15. Hsu A, Huntington KE, Carneiro BA, et al. Clinical activity of 9-ING-41, a small molecule selective glycogen synthase kinase-3 beta (GSK-3β) inhibitor, in refractory adult T-Cell leukemia/lymphoma. *Cancer Biol Ther*. 2022;23(1):417–423. doi:10.1080/15384047.2022.2088984
16. Shao R, Liu C, Xue R, Liu W, et al. Tumor-derived exosomal ENO2 modulates polarization of tumor-associated macrophages through reprogramming glycolysis to promote progression of diffuse large B-cell lymphoma. *Int J Biol Sci*. 2024;20(3):848–863. doi:10.7150/ijbs.91154
17. Tam BY, Chiu K, Chung H, et al. The CLK inhibitor SM08502 induces anti-tumor activity and reduces Wnt pathway gene expression in gastrointestinal cancer models. *Cancer Lett*. 2020;473:186–197. doi:10.1016/j.canlet.2019.09.009
18. Zhao X, Ren Y, Lawlor M, et al. BCL2 amplicon loss and transcriptional remodeling drives ABT-199 resistance in B cell lymphoma models. *Cancer Cell*. 2019;35(5):752–766.e9. doi:10.1016/j.ccell.2019.04.005
19. Kang X, Wang H, Li Y, et al. Alantolactone induces apoptosis through ROS-mediated AKT pathway and inhibition of PINK1-mediated mitophagy in human HepG2 cells. *Artif Cells Nanomed Biotechnol*. 2019;47(1):1961–1970. doi:10.1080/21691401.2019.1593854
20. Naderi R, Gholizadeh-Ghaleh Aziz S, Haghigi-Asl AS. Evaluating the effect of alantolactone on the expression of N-cadherin and vimentin genes effective in epithelial-mesenchymal transition (EMT) in breast cancer cell line (MDA-MB-231). *Ann Med Surg Lond*. 2022;73:103240. doi:10.1016/j.amsu.2021.103240
21. Sun X, Xu H, Dai T, et al. Alantolactone inhibits cervical cancer progression by downregulating BMI1. *Sci Rep*. 2021;11(1):9251. doi:10.1038/s41598-021-87781-z
22. Ding Y, Gao H, Zhang Y, et al. Correction to: alantolactone selectively ablates acute myeloid leukemia stem and progenitor cells. *J Hematol Oncol*. 2021;14(1):61. doi:10.1186/s13045-021-01069-3
23. He W, Cao P, Xia Y, et al. Potent inhibition of gastric cancer cells by a natural compound via inhibiting TrxR1 activity and activating ROS-mediated p38 MAPK pathway. *Free Radic Res*. 2019;53(1):104–114. doi:10.1080/10715762.2018.1558448
24. Yu X, Liao B, Zhu P, et al. β-caryophyllene induces apoptosis and inhibits cell proliferation by deregulation of STAT-3/mTOR/AKT signaling in human bladder cancer cells: an in vitro study. *J Biochem Mol Toxicol*. 2021;35(10):e22863. doi:10.1002/jbt.22863
25. Zhao W, Zhang Y, Wang L, et al. Adapalene inhibits prostate cancer cell proliferation in vitro and in vivo by inducing DNA damage, S-phase cell cycle arrest, and apoptosis. *Front Pharmacol*. 2022;13:801624. doi:10.3389/fphar.2022.801624
26. Rafique A, Muhammad S, Iqbal J, et al. Exploring the inhibitory potential of novel piperidine-derivatives against main protease (M(pro)) of SARS-CoV-2: a hybrid approach consisting of molecular docking, MD simulations and MMPBSA analysis. *J Mol Liq*. 2023;382:121904. doi:10.1016/j.molliq.2023.121904
27. Burley SK, Berman HM, Kleywegt GJ, et al. Protein data bank (PDB): the single global macromolecular structure archive. *Methods Mol Biol*. 2017;1607:627–641.
28. Kim S, Thiessen PA, Bolton EE, et al. PubChem substance and compound databases. *Nucleic Acids Res*. 2016;44:D1202–D1213. doi:10.1093/nar/gkv951
29. Wang DD, Ou-Yang L, Xie H, et al. Predicting the impacts of mutations on protein-ligand binding affinity based on molecular dynamics simulations and machine learning methods. *Comput Struct Biotechnol J*. 2020;18:439–454. doi:10.1016/j.csbj.2020.02.007
30. Slater O, Miller B, Kontoyianni M. Decoding protein-protein interactions: an overview. *Curr Top Med Chem*. 2020;20:855–882. doi:10.2174/1568026620666200226105312
31. Zhang R, Chen Y, He J, et al. WGCNA combined with GSVA to explore biomarkers of refractory neocortical epilepsy. *IBRO Neurosci Rep*. 2022;13:314–321. doi:10.1016/j.ibneur.2022.09.010
32. Zhao X, Zhang L, Wang J, et al. Identification of key biomarkers and immune infiltration in systemic lupus erythematosus by integrated bioinformatics analysis. *J Transl Med*. 2021;19:35. doi:10.1186/s12967-020-02698-x
33. Wu DW, Huang CC, Chang SW, et al. Bcl-2 stabilization by paxillin confers 5-fluorouracil resistance in colorectal cancer. *Cell Death Differ*. 2015;22(5):779–789. doi:10.1038/cdd.2014.170
34. Campos MS, Rodini CO, Pinto-Júnior DS, et al. GAPD and tubulin are suitable internal controls for qPCR analysis of oral squamous cell carcinoma cell lines. *Oral Oncol*. 2009;45(2):121–126. doi:10.1016/j.oraloncology.2008.03.019
35. Ren Y, Bi C, Zhao X, et al. PLK1 stabilizes a MYC-dependent kinase network in aggressive B cell lymphomas. *J Clin Invest*. 2018;128(12):5517–5530. doi:10.1172/JCI122533
36. Rodon J, Argilés G, Connolly RM, et al. Phase 1 study of single-agent WNT974, a first-in-class Porcupine inhibitor, in patients with advanced solid tumours. *Br J Cancer*. 2021;125:28–37. doi:10.1038/s41416-021-01389-8
37. Khan RB, Patay Z, Klimo P, et al. Clinical features, neurologic recovery, and risk factors of postoperative posterior fossa syndrome and delayed recovery: a prospective study. *Neuro Oncol*. 2021;23:1586–1596. doi:10.1093/neuonc/noab030
38. Liu P, Hang X, Li J, et al. Chidamide represses MYC expression and might improve survival for patients with double expressor lymphoma. *Am J Cancer Res*. 2024;14(6):2921–2933. doi:10.62347/GIIR3351
39. Abramson JS, Geyer SM, Pederson LD, et al. Randomized phase II/III study of R-CHOP ± venetoclax in previously untreated MYC/BCL2 double expressor diffuse large B cell lymphoma (DLBCL): alliance A051701 [abstract].